Astron. Astrophys. 318, 19–28 (1997)

ASTRONOMY AND ASTROPHYSICS

The anatomy of an isolated spiral galaxy: NGC 4414

J. Braine[1], **N. Brouillet**[2], **and A. Baudry**[2]

[1] IRAM, 300, rue de la Piscine, F-38406 St. Martin d'Hères, France
[2] Observatoire de Bordeaux, URA 352, CNRS/INSU, B.P. 89, F-33270 Floirac, France

Received 24 April 1996 / Accepted 26 June 1996

Abstract. Our on-going observations of the interstellar medium of NGC 4414 have resulted in CO(1–0) and CO(2–1) detections to very close to the optical edge of the disk. The ^{13}CO lines and thermal dust continuum emission have been detected almost as far out. The variation in the beam-independent CO($\frac{2-1}{1-0}$) line intensity ratio is interpreted in terms of a variation in the CO excitation temperature. Combining the temperature variation with the galactic size-linewidth relation and the virial theorem enables us to estimate how the $N(\mathrm{H_2})/I_{\mathrm{CO}}$ factor varies as a function of galactocentric radius. One then straightforwardly obtains the distribution of the molecular gas. It should be noted that because there is probably little or no star formation and neutral gas in the nucleus of NGC 4414, we avoid problems associated with conditions proper to galactic nuclei but thus make no predictions for these regions.

In order to check the $N(\mathrm{H_2})/I_{\mathrm{CO}}$ function obtained above, we used our ^{13}CO (1–0) and ^{13}CO (2–1) data, in conjunction with the ^{12}CO and assuming the ^{13}CO to be optically thin, to derive absolute ^{13}CO abundances as a function of radius. The resulting abundances are in good agreement with galactic observations. The millimeter-wave thermal emission from dust is a second independent test. While grain cross-sections and, to a lesser extent, dust temperatures are subject to debate, commonly used values yield gas masses quite close to those we estimate from our analysis. Unusually low cross-sections or temperatures and a peculiar variation are required to fit the gas mass resulting from the use of a constant $N(\mathrm{H_2})/I_{\mathrm{CO}}$ ratio. All of our observations support the variation and range of $N(\mathrm{H_2})/I_{\mathrm{CO(1-0)}}$ that we propose here for NGC 4414. It should however be borne in mind that a number of assumptions about molecular clouds have been made and that we have no means of verifying them for the clouds in NGC 4414.

As such an analysis is not yet available for other external spiral galaxies, we have applied our knowledge of the gas and stellar distributions to the question of what controls star formation on large scales. NGC 4414 is an ideal test case because of its inner and outer cutoffs in the HII region distribution and because it has probably not suffered tidal interactions with other galaxies recently. We find that both cutoff radii are well reproduced using the simple Q criterion for gravitational instability.

Key words: galaxies: abundances – galaxies: evolution – galaxies: individual NGC 4414 – galaxies: ISM – galaxies: spiral – radio lines: galaxies

1. Introduction

Although 20 years have gone by since the first extragalactic CO detection (Rickard et al. 1975), our knowledge about the molecular content of the outer regions of the disks of spiral galaxies remains quite unsatisfying. Early extragalactic observations lacked the necessary sensitivity and more recent work has focussed on the bright inner disks. The development of mm-wave interferometers has only increased this disparity as weak extended sources, such as the outer regions of disks, are inappropriate targets. Galactic surveys (Sanders et al. 1984; Cohen et al. 1986; Terebey et al. 1986; Dame et al. 1987) provided useful medium-sensitivity information about ring and outer disk clouds. More recently, Brand & Wouterloot (1995) and Digel et al. (1994) made more detailed observations of the CO content of the outer Galaxy and the relationship between the CO and HI, which was always found near the molecular clouds. The main difference is the lower CO luminosity of the distant clouds (Terebey et al. 1986; Mead & Kutner 1988; Digel et al. 1994).

We are still unable to answer, even in an approximate way, some very basic questions about spiral galaxies.
— What fraction of the molecular gas is beyond $R_{25}/2$ and beyond R_{25}? How can its mass be measured? Is there a "standard" distribution of molecular gas in spiral disks?
— How do average cloud properties such as temperature, volume density, and column density, vary with galactocentric distance ? How do the abundances of basic molecules and dust vary with radius? — What determines the rate of star formation – gas density, overall galactic dynamics, thresholds ...? The goal of this paper is to go as far as possible in this direction for a single galaxy. More precisely, we want to use our detailed molecular line data to assess the large-scale temperature variations. This will then be used to derive a variable $N(\mathrm{H_2})/I_{\mathrm{CO}}$ factor and

Send offprint requests to: Jonathan Braine

thus the distribution of molecular gas out to close to the optical radius.

We have chosen to study the outer disk of the fairly isolated, late-type, flocculent, galaxy NGC 4414. Gravitational encounters are known to affect the distribution of matter in galaxies (e.g. Toomre & Toomre 1972) and particularly the gaseous component (e.g. Barnes & Hernquist 1991). Therefore, we want to avoid this effect as much as possible by choosing a galaxy with no close neighbors. The fact that the diffuse atomic gas is extremely extended (to more than twice the optical limits) is further evidence in favor that NGC 4414 has not been subjected to significant tidal forces from other galaxies. Simulations show that encounters and mergers can change the classification of a galaxy but only in one direction – towards earlier types. Late-type spirals (Sc) are also the most common and thus should be the most representative. A flocculent galaxy is a galaxy with poorly defined spiral arms, the opposite of a grand-design spiral such as M 51 (cf.Elmegreen & Elmegreen 1982,1987). Flocculent systems are much more common and more axi-symmetric than the grand-design spirals so they are better representatives of the "average" spiral. The lack of large-scale structure makes an axi-symmetric approximation (simplification) acceptable.

NGC 4414 seemed an excellent, although clearly not unique, candidate given these criteria. Braine, Combes, & van Driel (1993; hereafter Paper I) mapped most of the galaxy in ^{12}CO (1–0) and ^{12}CO (2–1) and out to nearly half the optical radius R_{25} (108″, de Vaucouleurs et al. 1991) in ^{13}CO (1–0) and ^{13}CO (2–1). In this paper we incorporate even more extensive observations in all four lines and the combined data set forms the basis for our analysis along with the HI observations with the Westerbork interferometer presented in Paper I.

The recession velocity of NGC 4414 is $v_{\rm hel}$ = 716 km s^{-1} and the distance adopted here for all calculations is 9.6 Mpc. The linear scale is therefore 21″ per kpc. NGC 4414 has been observed in four CO lines over nearly the whole disk and we intend to use this to go further, with one galaxy, than has been previously done to answer the above questions. Sect. 2 briefly describes the observations and data reduction. In Sect. 3, we develop a model for the CO distribution which, in Sect. 4, is used to assess the variation of the temperature with radius. This is then used to compute an appropriate $N({\rm H_2})/I_{\rm CO}$ factor. Some HCN(1–0) observations (made by us in 1992) are discussed in Sect. 5 in terms of their relevance to the $N({\rm H_2})/I_{\rm CO(1-0)}$ conversion factor. Sect. 6 addresses the H_2 distribution and in Sect. 7 we derive ^{13}CO abundances which we compare with estimates for the Milky Way as no such determinations are available for other galaxies. We then try to address the central question of how the rate of star formation is controlled. Models are compared with the observational results in Sect. 8.

2. Observations and data reduction

All molecular line observations presented here come from the 30 meter telescope at Pico Veleta (Spain) run by the Institut de Radio Astronomie Millimétrique (IRAM). The first set of observations was taken in August 1991 and is described in Paper I. The new CO line data set (^{12}CO (1–0), ^{12}CO (2–1), ^{13}CO (1–0), and ^{13}CO (2–1)) was obtained from June 13 to June 17, 1994 and concerns essentially the outer parts of the galaxy. The HCN(1–0) line (88.6 GHz) was also observed under poor sky conditions in May 1992.

Simultaneous observation of the 1-0 and 2-1 transitions was possible in both isotopes with the 3mm and the two 1mm SIS receivers, two filterbanks of 512 × 1 MHz channels, and the autocorrelator in various configurations. Cross-calibration with the previous observations and by directing the signals into several backends simultaneously, showed that the "first" filterbank, usually called B30, was defective and underestimated the antenna temperature by a factor close to 2. It was subsequently disconnected. It is not known when the problem started so data obtained with the B30 backend shortly before June 13, 1994 should be examined carefully.

Pointing was checked every 60 to 120 minutes on the quasars 3C273 and 1308+326 and found to be accurate to $\lesssim$ 3″ rms. The calibration in intensity was checked on NGC 4414 itself for the ^{12}CO line and by observing SgrB2(M) for the ^{13}CO line (where the SO line was observed at roughly the frequency of the redshifted ^{13}CO). System temperatures varied from 200 K to 300 K (T_a^* scale) at 110 and 115 GHz and from 300 K to 700 K at 220 and 230 GHz. Cold load calibrations were made every 4 or 8 minutes integration time as a function of receiver and atmospheric stability.

The data were reduced with the CLASS software and the June 1994 data were combined with the August 1991 observations presented in Paper I.

3. Radial distribution of CO emission

Assuming a position angle of 30°and an inclination of 56°, the combined data set was rotated such that the major axis is parallel to the y-axis and deprojected in order to obtain a radial distribution of the CO intensity in all 4 lines.

Based on the Hα hole (see image in Pogge 1989) and on the results of Paper I, we adopted a distribution consisting of a central hole of radius $r_{\rm min}$ = 4″, void of CO emission, followed by a plateau, followed by an exponential disk. Several other distributions were also tested but provided much poorer fits to the data.

$$\begin{aligned} I_{\rm CO} &= 0 \qquad\qquad (r < r_{\rm min}) \\ &= I_{\rm plat} \qquad (r_{\rm min} \le r \le r_{\rm plat}) \\ &= I_{\rm plat}\, exp((r_{\rm plat} - r)/r_0) \quad (r > r_{\rm plat}) \end{aligned} \tag{1}$$

Fitting the observational data with Eq. 1 convolved with a gaussian beam response of the appropriate size (taken to be 12″ for the $J = 2 - 1$ transition and 23″ for the $J = 1 - 0$ transition), we obtained a plateau size of 28″ for both the ^{12}CO (1–0) and ^{12}CO (2–1) data sets (see Fig. 1 and Table 1). The ^{13}CO data also fit the same solutions but fewer positions, about 35% as many, are available for the ^{13}CO lines. The exponential scale

Table 1. Fit parameters for CO distribution

	central hole	plateau	exponential disk
CO(1–0)	$r_{\rm min}$ = 4″	$r_{\rm plat}$ = 28″	r_0 = 17″
CO(2–1)	$r_{\rm min}$ = 4″	$r_{\rm plat}$ = 28″	r_0 = 15″

length was estimated to be 17″ for the ^{12}CO (1–0) and 15″ for the ^{12}CO (2–1). As these results are obtained for the assumed distribution after convolution with the beam, the difference in exponential scale length cannot be attributed to the difference in beam sizes. The same modeling was done for the HI but clearly with different parameters. The advantage in carrying out such modeling is that one obtains smoothly varying, beam-independent brightnesses. The distribution described above, along with the observed CO and HI rotation curves from Paper I, forms the basis for the following analysis. No attempt has been made to produce a non-axi-symmetric distribution because of (i) the lack of obvious spiral arms and (ii) the insufficient angular resolution of the CO and HI observations.

4. Temperature variation as a function of radius

While subject to all the usual caveats about the molecular cloud structure, the intensity ratio of the CO(2–1) and CO(1–0) lines, ICO($\frac{2-1}{1-0}$), should give us some information about the variation in excitation temperature, especially if the values are relative rather than absolute.

Defining

$$CO(\frac{2-1}{1-0}) = \frac{J(\nu_{21}, \alpha\, T_{ex}) - J(\nu_{21}, T_{bg})}{J(\nu_{10}, T_{ex}) - J(\nu_{10}, T_{bg})} \qquad (2)$$

where $J(\nu, T) = \frac{h\nu}{k}(exp(h\nu/(kT)) - 1)^{-1}$ and where ν_{10} and ν_{21} are the frequencies of the CO(1–0) and CO(2–1) lines. Multiplying the excitation temperature $T_{\rm ex}(1-0)$ by α is meant to take into account the slightly subthermal excitation of the higher transition. The line intensity ratio ICO($\frac{2-1}{1-0}$) $\approx$ 0.7 in the central arcminute of NGC 4414 is typical of galactic disks. We make the hypothesis that the parameter alpha remains roughly constant although it is sensitive to the level of radiative excitation. In support of this hypothesis we note that radiative excitation increases only very slowly at high optical depths and that in giant molecular clouds, which appear to make up most of the molecular gas mass, both ^{12}CO lines are highly optically thick. We further assume that there is no difference in "filling factors" between the two transitions. In our analysis, α is taken to be constant with radius so any variation of ICO($\frac{2-1}{1-0}$) is due to excitation temperature changes. These, in turn, are likely to be the result of changes in the thermal temperature although the equation $T_{ex} = T_{kin}$ may not be correct.

In order to do this, we use the beam-independent distributions determined in Sect. 3 to calculate ICO($\frac{2-1}{1-0}$) as a function of position. In Fig. 1, we show the observed intensities in the ^{12}CO lines (crosses), the fit from Sect. 3 convolved to the appropriate beamsize and for an inclination of 56° (solid line) and the values for the fit with no convolution (boxes). No fit is perfect given the scatter but we feel that the agreement is quite good, especially given that the form of the fit was not inspired by the CO observations but by the Hα. It is also readily apparent that at radii greater than 40″ there is no need for convolution.

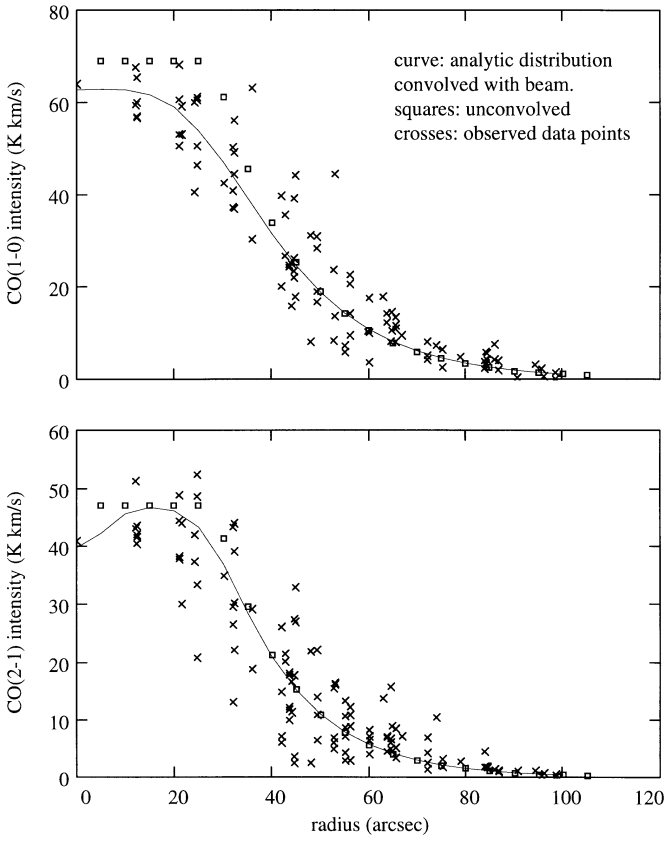

Fig. 1. Comparison of observed CO intensities (crosses) with model distribution (open squares) and model distribution convolved to the resolution of the observations (solid line) versus radius in arcseconds. Top frame is for the CO(1–0) line and bottom for CO(2–1). In the CO(1–0) line, rms errors are smaller than the symbol size ($<$ 2 K km s^{-1}), and much smaller where the intensity is low. The uncertainties in the CO(2–1) line are roughly twice as large.

We have inverted Eq. (2) to give temperatures as a function of the line ratio. The adopted value for α is 0.85, corresponding to a ^{12}CO (1–0) excitation temperature of about 17 K decreasing to about 6 K from the inner to outermost regions. The line ratio decreases from about 0.7 in the central regions to about 0.45 at a radius of 80″. Direct comparison of the CO(2–1) and CO(1–0) lines point by point yields a ratio of about 0.7 out to about 40″ or 50″ followed by a drop to about 0.4 - 0.5 at radii of 80″ or greater so nothing artificial seems to have been introduced by our methods. For the rest of this work, we focus on the smooth beam-independent intensities for all calculations. Errors become significant at radii above 80″ and very little use is made of the molecular gas distribution beyond the furthest detection ($\sim$ 100″, slightly below the optical radius R_{25} = 108″).

Fig. 2 shows the variation of the ^{12}CO (1–0) excitation temperature with radius. Increasing α would decrease the temper-

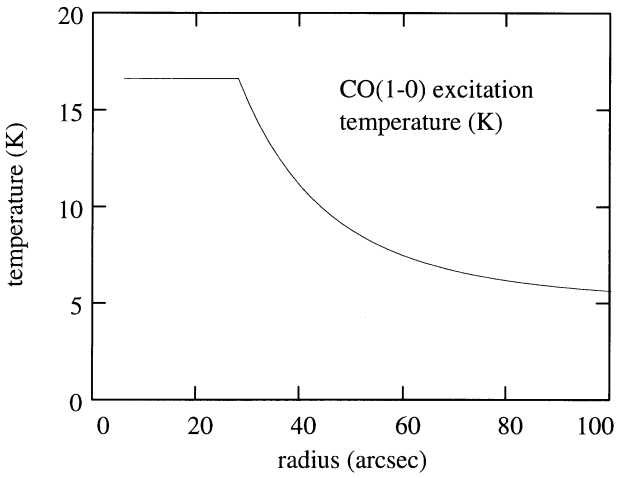

Fig. 2. ^{12}CO (1–0) excitation temperature (ordinate, in Kelvin) as a function of radius (abscissa, in arcseconds) for α = 0.85.

ature. If $\alpha > 0.9$, then the excitation temperature would have to be $T_{ex} < 10$ K for ^{12}CO (1–0), which is below typically observed temperatures in the ^{12}CO (1–0) line for inner Galaxy clouds. If $\alpha < 0.8$, then the excitation temperature would have to be $T_{ex} > 25$ K, which is certainly above standard Galactic values. $\alpha \approx 0.85$ also yields a conservative estimate of temperature variations with radius. If α were lower (i.e. 0.8), then the decrease in temperature with radius would be sharper.

With α = 0.85, the temperature decreases by a factor 2 as ICO($\frac{2-1}{1-0}$) decreases from $\sim$ 0.7 to $\sim$ 0.5. The temperature undoubtedly plays a role in determining the amount of CO emission per unit of molecular hydrogen – the $N(H_2)/I_{CO(1-0)}$ factor used to estimate molecular gas masses from CO observations of galaxies – so we will try to use this information to determine the radial distribution of N_{H_2}.

5. Dense gas tracers

In May of 1992 we observed the HCN(1–0) line in below average conditions. Several positions were observed along the major axis and the typical intensity ratio is $I_{CO(1-0)}/I_{HCN(1-0)} \approx 40$. This is normal for gas-rich spirals but an order of magnitude lower than in ultraluminous FIR galaxies (Solomon et al. 1992) and a factor of a few below the central regions of the starburst galaxies M 82 and NGC 253 (Nguyen-Q-Rieu et al. 1989). Despite its high gas surface density, NGC 4414 is by no means a starburst galaxy (additional reasons given in Paper I).

One of the reasons for observing HCN or other tracers of dense gas is that the $N(H_2)/I_{CO(1-0)}$ factor probably depends on volume density (among other dependencies). A particularly high (low) $I_{HCN(1-0)}/I_{CO(1-0)}$ would suggest unusually dense (diffuse) gas and thus a higher (lower) $N(H_2)/I_{CO(1-0)}$ factor. The fact that a typical value has been observed suggests that the calculations below are reasonable, at least with respect to the gas density.

6. $N(H_2)/I_{CO(1-0)}$ and the radial distribution of N_{H_2}

Several methods have been used to try to determine the $N(H_2)/I_{CO}$ ratio (see Combes 1991 for a review) in the Milky Way and there is general agreement that the factor probably increases with radius. However, in observations of external galaxies a non-varying factor has always (to our knowledge) been used to estimate H_2 masses. Three general regions can be identified: the galactic center, the molecular disk, and the outer galaxy. The clouds themselves may have a different structure in the galactic center due to the strong tidal forces and this may well invalidate the "Virial theorem based" $N(H_2)/I_{CO(1-0)}$ calibration in this region. Virial calculations assume that only internal factors govern the line-width and not large-scale dynamical processes in the galaxy. One of the reasons for our choice of NGC 4414 for this study is that there is probably extremely little molecular gas in the nucleus, eliminating the problem of galactic center cloud structure and temperature.

The observed size-linewidth relationship for disk clouds (Larson 1981; Myers 1983; Sanders et al. 1985; Solomon et al. 1987), injected into the Virial theorem (i.e. the assumption that clouds are bound and relatively stable), provides a means of determining $N(H_2)/I_{CO(1-0)}$ as a function of temperature and cloud size. Such calculations were performed by Dickman et al. (1986) and we rapidly present similar calculations below in order to illustrate the dependence on the observed and derived quantities.

A number of authors have suggested that the observed size-linewidth relationship does not necessarily imply gravitational equilibrium (*e.g.* Issa et al. 1990; Maloney 1990) and cannot be combined with a purely gravitational Virial theorem to deduce cloud masses. It is clear that clouds do not collapse in times of the order of the free-fall collapse time (*e.g.* Zuckerman & Palmer 1974) and little if any evidence exists for large-scale collapse. We use it here given its apparent success when compared to other $N(H_2)/I_{CO}$ calibrations keeping in mind that it is likely an upper limit to the real cloud mass. For a saturated line, like ^{12}CO (1–0), the Virial theorem gives a cloud mass of

$$M_{cl} \approx \frac{\Delta V^2 \, (4 A_{cl}/\pi)^{1/2}}{2\,\gamma\,G} \tag{3}$$

where .5 $\lesssim \gamma \lesssim$ 2 (e.g. Dickman et al. 1986). M_{cl} and A_{cl} are respectively the mass and projected area of the cloud, ΔV is the half power line width of the cloud. This translates into

$$\begin{aligned} N(H_2)/I_{CO(1-0)} &\approx \frac{M_{cl}\, f_H}{A_{cl}\, T_{10}\, \Delta V\, 2 m_p} \\ &\approx \frac{\Delta V\, f_H}{2\sqrt{\pi}\, m_p\, \gamma\, G \sqrt{A_{cl}}\, T_{10}} \end{aligned} \tag{4}$$

where f_H is the hydrogen fraction by mass (f_H = 0.73: Allen 1991, assumed to be molecular). To go from M_{cl} to $N(H_2)/I_{CO(1-0)}$ we have assumed that $M_{cl} \propto A_{cl} \propto \Delta V^4$ with ΔV = 1 km s^{-1} corresponding to A_{cl} = 1 pc^2. It should be noted that Virial masses depend on the velocity structure within

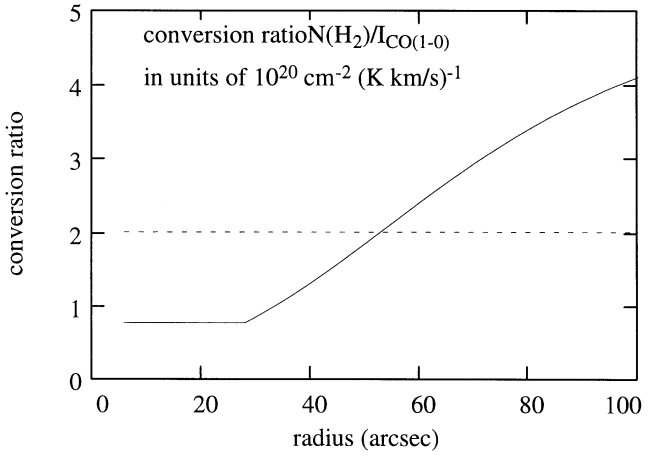

Fig. 3. $N(\mathrm{H_2})/I_{\mathrm{CO}(1-0)}$ (ordinate, in $\mathrm{H_2\,cm^{-2}(\,K\,km\,s^{-1})^{-1}}$) as a function of radius (abscissa) for $\gamma = 2$ $\beta = 1.58$ (see Eq. 4 and Sect. 6). and the temperature variation from Fig. 2. ^{12}CO is assumed to be highly optically thick. The dotted line corresponds to a rather "standard" value for $N(\mathrm{H_2})/I_{\mathrm{CO}(1-0)}$.

the cloud and should not be considered to be precise to better than about 50%.

One of the problems in such calculations is how cloud size is defined. Compared to Solomon et al. (1987), our cloud line widths appear somewhat narrower, closer to those of Myers (1983), but the total cloud mass as a function line width is identical. The most important quantity to compare is the cloud averaged surface density which, in our model, is half that obtained by Solomon et al. However, as stated above, we have deliberately tried to err towards lower cloud masses because we view Solomon et al.'s values as upper limits. Our values are very close to those of Dickman et al. (1986).

In this way, a value can be obtained for a given cloud size or, integrating over all clouds, for an ensemble. Sanders et al. (1985) determined a mass spectrum for the Milky Way disk of $n(m) \propto m^{-\beta}$ with $\beta = 1.58$. This can be converted into a velocity width spectrum and integrated, yielding $N(\mathrm{H_2})/I_{\mathrm{CO}(1-0)}$ as a function of temperature. As long as $\beta < 2$, the mass spectrum is dominated by the massive clouds. Thus, the lower integration limit is not important but the upper limit affects the resulting conversion factor.

Fig. 3 illustrates the variation in $N(\mathrm{H_2})/I_{\mathrm{CO}(1-0)}$ as a function of radius for $\gamma = 2$ and $\beta = 1.58$ and an upper integration limit of $\Delta V = 7\,\mathrm{km\,s^{-1}}$. For $\beta = 1.78$ the factor is a factor 2 higher and if $\beta = 1.38$ it is 25% lower. We therefore find a conversion ratio of $N(\mathrm{H_2})/I_{\mathrm{CO}(1-0)} \approx 10^{20}\,\mathrm{cm^{-2}(\,K\,km\,s^{-1})^{-1}}$ for an average temperature of 15 K. $\gamma = 2$ is used throughout the rest of this paper. The hydrogen fraction by mass has been taken to be $f_H = 0.73$ (Allen 1991).

The radial distribution of the neutral gas components is shown in Fig. 4. On the left-hand side of the figure, the bottom curve is the atomic gas surface density, followed by the surface density of molecular gas (including the He contained in the molecular clouds), the total neutral gas surface density, and finally the total neutral gas surface density obtained using a constant $N(\mathrm{H_2})/I_{\mathrm{CO}(1-0)} = 2\,10^{20}\,\mathrm{cm^{-2}(\,K\,km\,s^{-1})^{-1}}$ factor. The mass distribution $M(r < R)\,vs.\,R$ is shown in Fig. 5 for the atomic, molecular, and molecular (with $N(\mathrm{H_2})/I_{\mathrm{CO}(1-0)}$ constant) media.

It has been implicitly assumed in the above that clouds do not overlap in velocity along the line of sight. Any overlap or shadowing will cause the $\mathrm{H_2}$ column density to be underestimated if a CO-$\mathrm{H_2}$ conversion factor is used based, as above, on the lack of overlap. Such overlap would, of course, be undetectable in ^{12}CO because it is optically thick. If clouds overlap in velocity along the same line of sight, then all molecular gas masses and $N(\mathrm{H_2})/I_{\mathrm{CO}}$ values determined here from optically thick lines (^{12}CO) must be multiplied by $(1 - f_{\mathrm{abs}})^{-1}$ where f_{abs} is the fraction of the emission absorbed along the line of sight (*i.e.* for two clouds exactly covering each other, half of the total emission is absorbed so $f_{\mathrm{abs}} = .5$).

7. Checks on the varying $N(\mathrm{H_2})/I_{\mathrm{CO}(1-0)}$ value

We have detected the (basically) optically thin ^{13}CO (1–0) and ^{13}CO (2–1) lines out to $0.75R_{25}$. Furthermore, the continuum emission, mostly due to thermal dust, in NGC 4414 has been measured at 245 GHz (in prep.). In the following, we use the ^{13}CO and dust continuum data as an additional means of weighing our work against other mass determinations.

7.1. The ^{12}CO/^{13}CO ratio and ^{13}CO abundance

The ^{13}CO data set used here includes detections in both transitions out to $r > 0.7R_{25}$, further than in the vast majority of galaxies that have been observed in ^{12}CO. In paper I we showed that the intensity ratio I(^{12}CO)/I(^{13}CO), hereafter $^{12/13}$CO, is constant at a value of 9 over the inner ∼arcminute. If the ^{12}CO is optically thick ($\tau_{^{12}\mathrm{CO}} \gg 1$), then $^{12/13}$CO reflects the absolute optical depth of ^{13}CO (averaged over all lines of sight). Along with the temperature information, we can attempt to derive absolute ^{13}CO column densities and, from our derived $\mathrm{H_2}$ column density distribution, absolute ^{13}CO abundances.

Averaged over the clouds observed, the ^{13}CO column density is

$$\langle N_{^{13}\mathrm{CO}}\rangle \approx \frac{\int n(\Delta V)\,\Delta V^4\,N_{^{13}\mathrm{CO}}(^{12/13}\mathrm{CO},\Delta V,T_{\mathrm{ex}})\,d\Delta V}{\int n(\Delta V)\,\Delta V^4\,d\Delta V}. \quad (5)$$

From Sect. 6, expressing the distribution as $n(\Delta V)$ rather than $n(m)$ yields $n(\Delta V) \propto \Delta V^{3-4\beta}$. The ΔV^4 factor weights the number by the mass so Eq. (5) is equivalent to $\langle N_{^{13}\mathrm{CO}}\rangle \approx M_{\mathrm{tot}}^{-1}\Sigma M_{cl}N_{13_{cl}}$ where the sum is over all clouds and M_{cl} is the cloud mass and $N_{13_{cl}}$ the cloud column density in ^{13}CO. The ^{13}CO abundance is therefore

$$\chi_{^{13}\mathrm{CO}} \approx \frac{\langle N_{^{13}\mathrm{CO}}\rangle\,(1 - f_{\mathrm{abs}})}{N(\mathrm{H_2})_{\mathrm{cl}}} \quad (6)$$

where $N(\mathrm{H_2})_{\mathrm{cl}}$ is the column density of $\mathrm{H_2}$ averaged over the area of a cloud.

$^{12/13}$CO is constant with radius out to $r \gtrsim 0.5\,R_{25}$. At larger radii, there may be a marginal increase from 9 to ∼ 11 but

no sharp decrease in optical depth is observed. No more reliable value being available, we assume that $^{12/13}$CO = 9 in both transitions for all radii. We determine $N_{^{13}\rm CO}$ for each transition separately assuming local thermal equilibrium (at the excitation temperature derived) in order to calculate the partition function. The results are shown in Fig. 6 for the ^{13}CO (1–0) line (top curve), ^{13}CO (2–1) line (bottom curve), and the average. The fairly large difference clearly shows that ^{13}CO is not in LTE and that significant errors could be made if only one transition were available. For simplicity, we use the average value for the abundance calculations below. We find, for the inner regions,

$$\chi_{^{13}\rm CO} \approx (1 - f_{\rm abs})\, 1.8\, 10^{-6} \qquad (7a)$$

and for the outer regions

$$\chi_{^{13}\rm CO} \approx (1 - f_{\rm abs})\, 6\, 10^{-7}. \qquad (7b)$$

^{12}CO abundance determinations generally give values of order $N_{\rm CO}/N_{\rm H_2} \approx 5\, 10^{-5}$ for both dark clouds and at least some high latitude clouds (Magnani et al. 1988 and references therein) and perhaps a factor 2 higher in the molecular ring. Langer & Penzias (1990) measured the $^{12/13}$C ratio in the galactic center and in several points in the disk. Their values of 30 - 40 for the inner molecular ring increasing to 70 slightly beyond the solar circle are in reasonable agreement with the Henkel et al. (1982) values of 45 and 90. Thus, for the Milky Way, a variation of about a factor 4 is expected from the inner molecular ring to the solar circle or somewhat beyond, ranging from roughly $\chi_{^{13}\rm CO} \sim 2.5\, 10^{-6}$ to $\chi_{^{13}\rm CO} \sim 6\, 10^{-7}$, very similar to what is found here.

Based on the above Galactic values, we assume that half of the decrease in $\chi_{^{13}\rm CO}$ is due to a decrease in the metallicity and the other half to a decline in the $^{12/13}$CO isotopic abundance ratio. We thus find an average radial decrease in the metallicity of about 0.1 dex per kpc for radii of $1 - 4$ kpc. This is marginally steeper than the average in the Zaritsky et al. (1994) sample of spirals or the Milky Way (Wilson & Rood 1994; Shaver et al. 1983; Mihalas & Binney 1981 and references therein) but NGC 4414 is a smaller than average spiral in terms of radius, if the distance we have assumed is roughly correct. The metallicity gradient is well within the normal range of the samples mentioned above and follows naturally from our analysis.

7.2. Gas mass from thermal dust emission

The 245 GHz continuum observations will be presented in more detail in a future paper. After subtraction of the contributions from the ^{12}CO (2–1), ^{13}CO (2–1), synchrotron, and free -free emission, the thermal dust emission from the inner 45″, 65″, and 90″ is about 140 mJy, 200 mJy, and 240 mJy respectively. Further out, noise dominates any signal. In order to estimate the gas mass from the thermal dust emission, we need to know the dust temperature and the dust cross-section per H atom (or equivalently the absorption coefficient in cm^2 per gram of gas). A reasonable estimate of the temperature of the cool dust is 15 K. Although a decrease can be expected with radius, the dust temperature cannot vary enormously given the strong dependence of total IR luminosity on dust temperature. The advantage of long-wavelength observations is that, aside from measuring optically thin emission, the temperature dependence is greatly reduced (linear in the Rayleigh-Jeans regime). Different sources give significantly differing values for the absorption coefficients.

We assume a grain cross-section of $\sigma_H = 7.5\, 10^{-27}$ cm^{-2} per H atom at 245 GHz (λ = 1.22 mm: Krügel & Chini 1994; Pollack et al. 1994) for the inner regions and the Draine & Lee (1984) cross-section (1.6 times lower) for the outer regions. These values reflect the variation in metallicity in the disk. The temperature of the cool dust is, for lack of information, taken to be 15 K. Total gas masses of 10^9 M$_\odot$, $1.6\, 10^9$ M$_\odot$ and $2.1\, 10^9$ M$_\odot$ are obtained for radii less than 45″, 65″, and 90″ respectively. The Draine & Lee cross-sections have been shown to hold for the atomic component (Braine et al. 1995, 1996; Neininger et al. 1996), typically at large radii. Somewhat higher values may be obtained in dense environments below about 25 K (temperature at which mantles may evaporate – Léger et al. 1985) because both condensation of molecules onto grains and imperfect coagulation of grains into less dense (fluffy) grains would increase the grain cross-section.

Comparison with Fig. 5 shows that the agreement is quite good. We have not included a dust temperature variation here for lack of information. The fact that any change in the dust temperature should be small and decreasing with radius means that trying to include such a variation would not alter our conclusions in any way and would only accentuate the difference with respect to the results using a constant $N({\rm H_2})/I_{\rm CO}$ factor.

The dust-based gas masses are below what is obtained by using a standard $N({\rm H_2})/I_{\rm CO(1-0)}$ value. Either a very low cross-section or a very low temperature is required to obtain the gas mass determined from a constant $N({\rm H_2})/I_{\rm CO(1-0)}$ factor. Decreasing the constant $N({\rm H_2})/I_{\rm CO}$ by more than a factor 2 yields a rough fit to the dust data but would not reproduce the variation in $\chi_{^{13}\rm CO}$. However, if our measures of the dust emission are accurate, in order to reconcile the dust-based gas masses with any constant conversion factor, the dust temperature would have to *increase* with galactocentric radius. Such a temperature variation is opposite what is expected. From this, we infer that our masses are indeed reasonable and that the Virial relation adopted here does not significantly underestimate the mass of clouds.

7.3. Is $N({\rm H_2})/I_{\rm CO}$ sensitive to the metallicity in NGC 4414?

The metallicity of a galaxy is clearly linked to the expected $N({\rm H_2})/I_{\rm CO}$ ratio (Cohen et al. 1988; Rubio et al. 1991) and indeed it seems logical to expect that, all other things being equal, more CO per unit H$_2$ should yield a higher $I_{\rm CO}/N_{\rm H_2}$. For fairly small (factor few or less) variations in the metallicity, however, no observations exist which can clearly answer the question. In their simulations, Wolfire et al. (1993) concluded that small variations, of the type we suggest for NGC 4414, should not have a significant effect on the $N({\rm H_2})/I_{\rm CO(1-0)}$ ratio.

We now try to use our formalism to address the question given our results for NGC 4414. The worry is whether a decrease in the metallicity Z would result in the CO being photodissociated more deeply into the clouds, thus reducing the apparent cloud size and the CO emission per unit H_2. The reduced CO column density might further lower the apparent cloud size because the point at which CO becomes optically thick could be driven deeper into the cloud. Conversely, one might also wonder whether the lower UV field in the outer regions would not allow the CO to remain intact even at larger distances from the cloud center. Or whether the decrease in excitation temperature would not increase the observed cloud size for low-J transitions. Naturally, the effects of such processes are highly dependent on cloud structure.

Assuming the CO forms chiefly at depths $A_v \gtrsim 0.5$ (van Dishoeck & Black 1988; Blitz et al. 1990), or $A_{uv} \gtrsim 2$, the dust is the major factor in determining the depth to which the CO is photodissociated. The dust abundance varies with Z. We expect therefore that the CO starts to form at a depth $d \propto F_{uv}/Z$ where F_{uv} is the strength of the ultraviolet radiation field near 1000Å. In order to estimate the observed cloud size (in CO), we will make the simplification that the "edge" of the cloud is where the optical depth τ of ^{12}CO is unity. As noted in Sect. 6, we assume that the mass-size-linewidth observed for the Galactic disk applies for the disk of NGC 4414 out to at least a radius of 4 kpc. The depth where $\tau_{\rm CO}$ = 1 is then determined by the excitation temperature and CO column density.

As stated in Sect. 7.1, we take $\chi_{^{12}\rm CO}(r) \propto Z(r) \propto \sqrt{\chi_{^{13}\rm CO}(r)}$, roughly -0.1 dex kpc^{-1}. The UV emission of spiral galaxies can probably be approximated as an exponential disk similar to that of the underlying stellar distribution (see figures in Buat et al. 1994), although there is likely more variation than for the optical emission. The optical scale length of the NGC 4414 disk is about 1 kpc or a decrease of roughly -0.4 dex kpc^{-1}. The variation of $Z(r)$ is clearly shallower so the depth to which CO is photodissociated may well decrease with galactocentric radius. For clouds which "see" a nearby ionizing star, the above calculation does not apply. Photodissociation is unlikely to significantly reduce cloud sizes at large galactocentric radii.

To estimate the depth at which $\tau_{\rm CO}$ = 1, we combine the temperature variation (Fig. 2) and the metallicity variation derived above in the standard formula for optical depth. Assuming LTE, we find that the cloud size should actually increase (i.e. the depth of the $\tau_{\rm CO}$ = 1 surface decreases: see solid curve in Fig. 7). In order to evaluate the depth for the case where few molecules are in high-J states, we have kept the partition function constant when determining where $\tau_{\rm CO}$ = 1. This gives the dashed curve in Fig. 7 and shows that in neither case does the apparent cloud size shrink.

All of these calculations have been done for simple centrally condensed clouds and may not be accurate for real clouds. We conclude that we see no evidence for a significant radial diminution in apparent cloud size due to a decrease in metallicity in NGC 4414, in accord with the Wolfire et al. (1993) study, although we have no means of excluding such effects for more complex clouds or if major changes in the cloud structure occur over the range in galactocentric radii studied here. The decrease in metallicity with radius is not expected to significantly affect the cloud temperature as long as most of the cooling is from optically thick lines (see Goldsmith & Langer 1978).

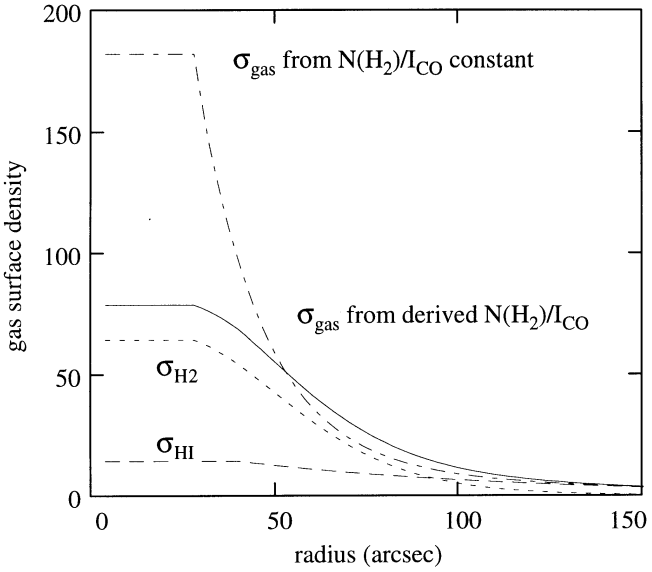

Fig. 4. Face-on distribution of the total gas surface density in $M_\odot$ pc^{-2} as a function of radius (arcseconds). The upper curve (dashed line) was determined using a constant $N(H_2)/I_{CO(1-0)}$ and the solid line with the derived $N(H_2)/I_{CO(1-0)}$. The molecular gas surface density alone (short dashed line) and the atomic gas surface density alone (long dashed line) are also plotted. The mass of Helium has been included in all cases.

8. Total gas surface density and star formation

As in many galaxies, the HI extends much further out than the CO emission. Using the $N_{H_2}(r)$ profile derived above and the HI observations from Fig. 15 of Paper I, we can derive the total gas surface density variation.

Tracing the gaseous content near the optical edges of spirals is clearly of interest to try to identify the reason for the apparent cutoff seen in many disks (Quirk 1972; van der Kruit & Searle 1981a, 1981b; Robin et al. 1992 and references therein). One of the standard explanations for the reduction in star formation is that the Toomre Q parameter (velocity dispersion over surface density) increases above a critical value near the optical edges of spirals (Kennicutt 1989), thus inhibiting further star formation. As pointed out by van der Kruit & Searle (1982), the Toomre (1964) and Goldreich & Lynden-Bell (1965) Q-criterion "provides no detailed prediction of $R_{\rm max}$ (the cutoff)".

8.1. The Q-criterion as a function of radius

For the gas component, Q is defined as (Toomre 1964; Binney & Tremaine 1987):

$$Q = \frac{v_{\rm gas}\,\kappa}{\pi\,G\,\Sigma_{\rm gas}} \qquad (8)$$

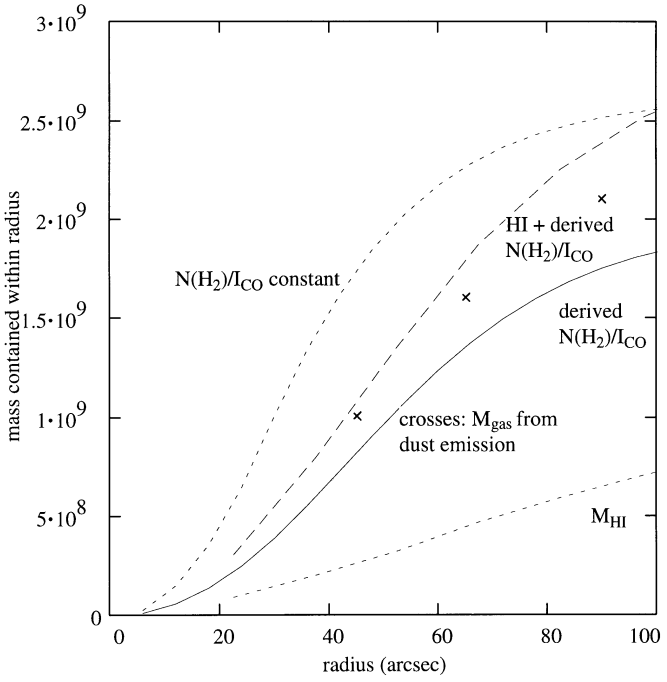

Fig. 5. Gas mass $M(r < R)$ in solar masses as a function of R (arcseconds). Top curve is H_2 (constant $N(H_2)/I_{CO(1-0)}$), the solid curve is H_2 from our analysis, the bottom curve is the HI mass, and the long dashed curve is the H_2 plus the HI, to be compared with the dust-based gas masses. All masses have been multiplied by 1.36 to include the mass of He. Crosses indicate total gas masses derived from 1.22 mm continuum observations.

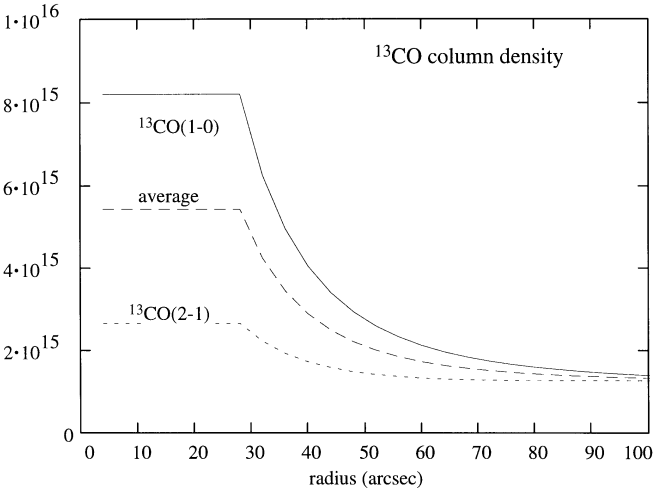

Fig. 6. ^{13}CO column density per cloud (molecules cm^{-2}) as a function of galactocentric distance (arcseconds). Top curve is for the ^{13}CO (1–0) line, bottom for ^{13}CO (2–1), and the middle curve is the average, which is what we adopt for the ^{13}CO column density.

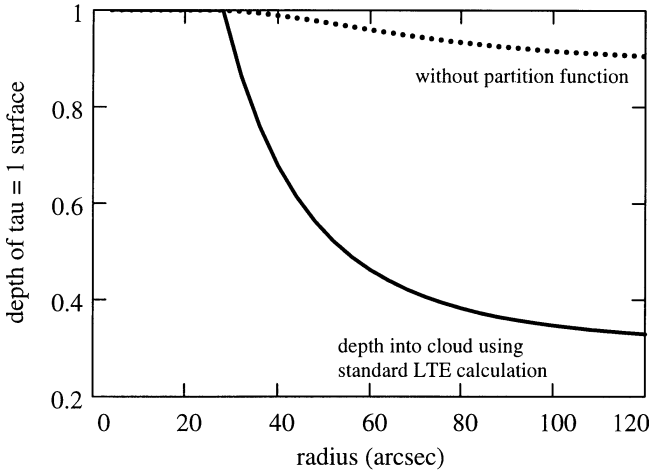

Fig. 7. Relative depth at which clouds become opaque in ^{12}CO (1–0). 1 is the value for inner galaxy (NGC 4414) clouds.

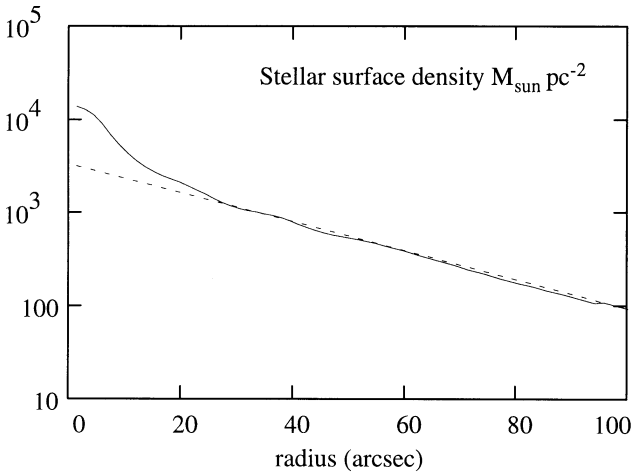

Fig. 8. Stellar surface density (face-on) in $M_\odot$ pc^{-2} as a function of radius (arcseconds). Dashed line represents the exponential disk.

where v_{gas} is the velocity dispersion of the gas, κ is the epicyclic frequency, and Σ_{gas} is the total gas surface density (see Cowie 1981, Jog & Solomon 1984a,b for much more detailed discussions). The epicyclic frequency can be estimated from the rotation curve. Σ_{gas} is based on our observations and has been amply discussed. The stellar mass surface density was derived from a red image of NGC 4414 (taken by W. van Driel with the Kiso Schmidt telescope), assuming a spherical bulge component and a thin inclined disk. The mass to light ratio was determined to be 8.6 $M_\odot / L_\odot$ from a "maximum disk" fit to the rotation curve. The results are shown in Fig. 8.

In Kennicutt's (1989) study, good agreement was obtained between the radius at which Q reached ∼1.6 (our definition) and the end of the HII region distribution. He did this work with much older, lower resolution CO(1–0) data using a constant $N(H_2)/I_{CO(1-0)}$ factor. Now that we have the necessary information, one of our goals was to test this for NGC 4414. NGC 4414 has the advantage of having both an inner ($\sim 20''$) and an outer ($\sim 70 - 90''$) radius for the HII region distribution (Pogge 1989; work in prep.).

In Fig. 9, we show the critical gas surface densities corresponding to $Q = 1$ and $Q = 1.6$ as well as the observed gas surface densities (see figure caption for details). It is immedi-

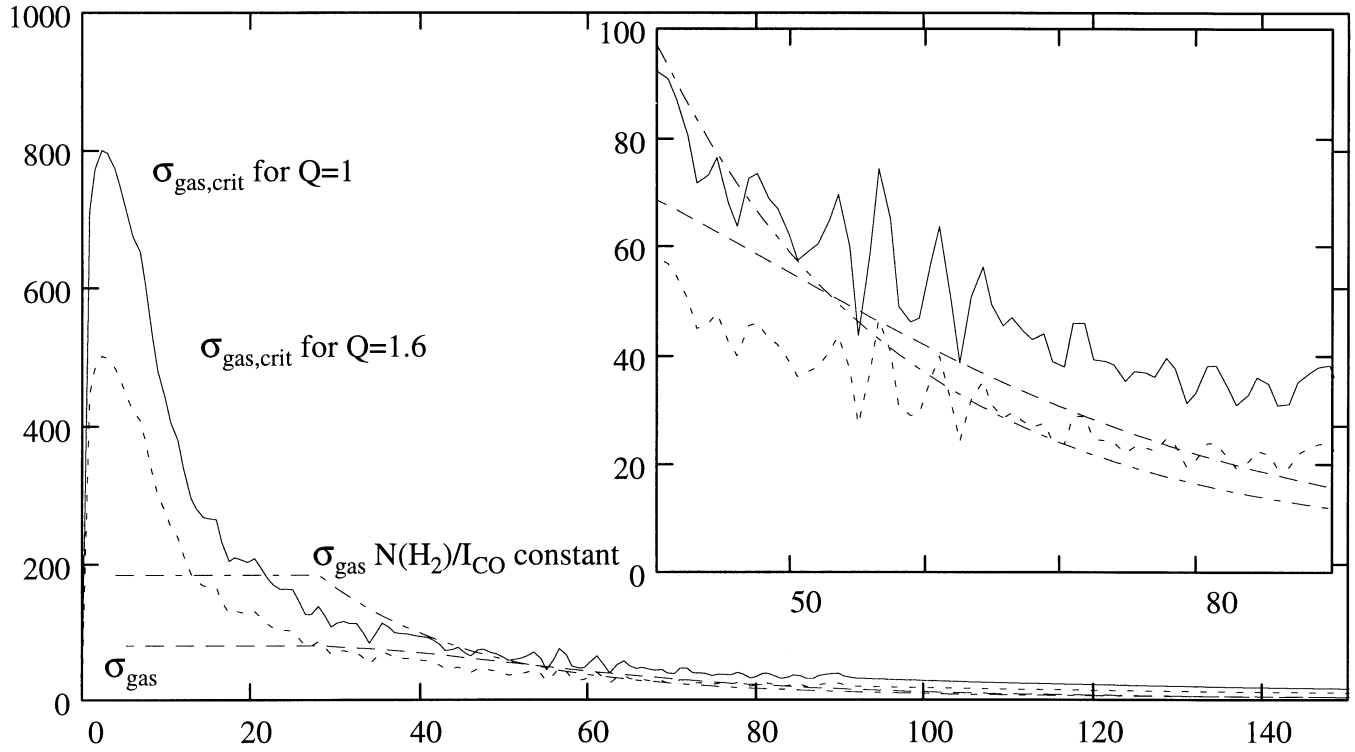

Fig. 9. Critical and observed gas surface densities (face-on) in $M_\odot$ pc^{-2} as a function of radius (arcseconds). Solid curve is the critical gas surface density for a Toomre Q parameter of 1 (see Eq. 8), short dashed line is for Q = 1.6 (best value found by Kennicutt 1989), dash-dot line is the observed gas surface density determined with a constant $N(\mathrm{H_2})/I_{\mathrm{CO}(1-0)}$ and the long dashed line is our adopted gas surface density.

ately clear that the radii for onset and cutoff of star formation determined for $Q \sim 1.6$ correspond quite well with the observed distribution of HII regions. One source of uncertainty, however, is the gas velocity dispersion, which has been assumed to be $v_{\mathrm{gas}} = 6 + 4exp(-\sqrt{r_{\mathrm{kpc}}})$ (cf. Dickey et al. 1990).

8.2. Other models

Elmegreen & Parravano (1994) argue that Q could remain low even in the outer regions. They propose a somewhat different mechanism to explain the presence of edges. In this scheme, star formation stops when the pressure is too low for normal compression events (*e.g.* turbulence, shock waves) to drive the gas into a low-temperature bound phase. If the pressure is too low, the gas will return to its original warm diffuse state. The appealing feature of this model is that it links the large-scale distribution with small-scale considerations (compression events and possible thermal equilibrium states). It could also explain why HI is observed much further out than molecular gas (although observational biases may be present as well).

We tried to apply their formulae to NGC 4414. We were not able to reproduce the inner cutoff and found that the outer cutoff could be made to vary greatly by changing the pressure, a poorly known parameter. While interesting, and perhaps quite appropriate for the outer edges of spirals, such models are not well constrained by current observables. We are not concerned here with models which attempt to reproduce correlations among galaxies, each considered as a single point.

The simplest prescription is that of Schmidt (1959) whereby the rate of star formation is simply proportional to some power of the local gas density. This was subsequently generalized to use a more readily observable parameter – the surface density. No single set of values for such a law fits the data well (see long discussions in Madore 1977 or Kennicutt 1989 and references therein). The fact that the gas distribution in spirals is frequently much more extended than the stellar distribution itself implies that a threshold should be included.

9. Conclusions

Our data support a radial gradient in the excitation temperature of the molecular gas with variations from temperatures of 15 − 20 K in the inner regions to 5 − 8 K near the optical radius R_{25}.

Assuming a size-line width-mass relation derived using the Virial theorem, we have estimated the value of the $N(\mathrm{H_2})/I_{\mathrm{CO}}$ conversion factor as a function of radius (from the temperature distribution) and then used this to determine the radial distribution of molecular gas. The estimates are corroborated by our maps in the ^{13}CO (1–0) and ^{13}CO (2–1) lines and 1.22 mm thermal continuum.

The data and analysis have been used to test two models of star formation thresholds in spiral disks – one based on the Toomre Q criterion and a more complex model based on the local gas pressure by Elmegreen & Parravano (1994). The Q model was found to fit the observations remarkably well, in

agreement with Kennicutt (1989). The model by Elmegreen & Parravano did not reproduce the inner star formation cutoff and, while roughly correct, the outer cutoff was highly dependent on poorly constrained observables. We found no empirical reason to look for an alternative to the Q based model.

Despite the relatively good agreement between theory and the different observational constraints, the calculations include several working assumptions which may prove not to be entirely valid. In particular, we have assumed that the decrease in the CO($\frac{2-1}{1-0}$) line ratio is due to a decrease in the excitation temperature of the molecular gas, that the clouds in the disk are "virialized" and that the Galactic size-linewidth relation can be applied to the clouds in the disk of NGC 4414. Our interpretation of the decrease in the CO($\frac{2-1}{1-0}$) ratio as a decrease in excitation temperature and the variation of $N(\mathrm{H_2})/I_{\mathrm{CO}}$ we deduce from it is essentially independent of the exact temperatures. It is clear, however, that our ignorance of the detailed cloud structure and illumination could have hidden other important causes for the decrease in the observed line ratio.

Acknowledgements. We wish to thank W. van Driel for the use of his red image and R. Pogge for the use of his full Halpha image of NGC 4414.

References

Allen, C.W., 1991, Astrophysical Quantities, The Athlone Press, London
Barnes, J., Hernquist L. 1991, ApJ 370, L65
Binney, J., Tremaine, S. 1987, *Galactic Dynamics* Princeton University Press, Princeton, New Jersey (USA).
Blitz, L., Bazell. D., Désert, F.X. 1990, ApJ 352, L13
Buat, V., Vuillemin, A., Burgarella, D., Milliard, B., Donas, J. 1994, A&A 281, 666
Braine, J., Combes, F., van Driel, W. 1993, A&A 280, 451. (Paper I)
Braine, J., Krügel, E., Sievers, A., Wielebinski, R. 1995, A&A 295, L55
Braine, J., Guélin, M., Dumke, M., Brouillet, N., Herpin, F., Wielebinski, R., 1996, A&A (in prep.)
Brand J., Wouterloot, J.G.A 1995, A&A 303, 851
Cohen, R.S., Dame, T.M., Thaddeus, P. 1986 ApJS 60, 695.
Cohen, R.S., Dame, T.M., Garay, G. et al. 1988, ApJ 331, L95
Combes F. 1991, ARAA 29, 195
Cowie, L.L. 1981, ApJ 245, 66
Dame, T.M., Ungerechts, H. Cohen, R.S. et al. 1987, ApJ 322, 706
Dickey, J.M., Hanson, M.M., Helou, G. 1990, ApJ 352, 522
Dickman, R.L., Snell, R.L., Schloerb, F.P. 1986, ApJ 309, 326.
Digel, S.de Geus, E., Thaddeus, P. 1994, ApJ 422, 92
van Dishoeck, E.F., Black J.H. 1988, ApJ 334, 711
Draine, B.T., Lee, H.M. 1984, ApJ 285, 89
Elmegreen D.M., Elmegreen B.G. 1982, MNRAS 201, 1021
Elmegreen D.M., Elmegreen B.G. 1987, ApJ 314, 3
Elmegreen B.G., Parravano, A. 1994, ApJ 435, L121.
Goldreich, P., Lynden-Bell, D. 1965, MNRAS 130, 7.
Goldsmith, P.F., Langer, W.D. 1978, ApJ 222, 881
Henkel, C., Wilson, T.L., Beiging, J. 1982, A&A 109, 344.
Issa, M., Maclaren, I., Wolfendale, A.W., 1990, ApJ 352, 132
Jog, C.J., Solomon, P.M. 1984a, ApJ 276, 114
Jog, C.J., Solomon, P.M. 1984b, ApJ 276, 127
Kennicutt, R.C. 1989, ApJ 344, 685.
Krügel, E., Chini, R. 1994, A&A 287, 947
Langer, W.D., Penzias, A.A. 1990, ApJ 357, 477.
Larson, R.B. 1981, MNRAS 194, 809.
Léger, A., Jura, M., Omont, A. 1985, A&A 144, 147
Madore, B.F. 1977, MNRAS 178, 1
Magnani, L., Blitz, L., Wouterloot, J.G.A. 1988, ApJ 326, 909.
Maloney, P. 1990, ApJ 348, L9
Mead, K.N., Kutner, M.L. 1988, ApJ 330, 399
Mihalas, D., Binney, J. *Galactic Astronomy*, Freeman, 1981
Myers, P.C. 1983, ApJ 270, 105
Neininger, N., Guélin, M., García-Burillo, S., Wielebinski, R. 1996, A&A (in press)
Nguyen-Q-Rieu, Nakai, N., Jackson, J.M. 1989, A&A 220, 57.
Pogge, R. 1989, ApJS 71, 433.
Pollack, J.B., Hollenbach, D., Beckwith, S. et al. 1994, ApJ 421, 615
Quirk, W.J. 1972, ApJ 176, L9
Rickard, L., Palmer, P., Morris, M., Zuckerman, B., Turner, B. 1975, ApJ 199, L75
Robin, A., Crézé, M., Mohan, V. 1992, A&A 26 5, 32.
Rubio, M., Garay, G., Montani, J., Thaddeus, P. 1991, ApJ 368, 173
Sanders, D.B., Solomon, P.M., Scoville, N.Z. 1984, ApJ 276, 182.
Sanders, D.B., Scoville, N.Z., Solomon, P.M 1985, ApJ 289, 373.
Schmidt, M. 1959, ApJ 129, 243
Shaver, P.A,, McGee, R.X., Newton, L.M., Danks, A.C., Pottasch, S.R. 1983, MNRAS 204. 53.
Solomon, P.M., Rivolo, A.R., Barrett, J., Yahil, A. 1987, ApJ 319, 730.
Solomon, P.M.,Downes, D., Radford, S.J.E. 1992, ApJ 387, L55.
Terebey, S., Fich, M., Blitz, L., Henkel, C. 1986, ApJ 308, 357.
Toomre, A. 1964, ApJ 139, 1217.
Toomre, A., Toomre, J. 1972, ApJ 178, 623
van der Kruit, P.C., Searle, L. 1981a, A&A 95, 105.
van der Kruit, P.C., Searle, L. 1981b, A&A 95, 116.
van der Kruit, P.C., Searle, L. 1982, A&A 110, 61.
de Vaucouleurs, G., de Vaucouleurs, A., Corwin, H.G. et al. 1991, *Third Reference Catalogue of Bright Galaxies*, Springer-Verlag, New York. (RC3)
Wilson, T.L., Rood, R.T. 1994, ARAA 32, 191
Wolfire, M.G., Hollenbach, D., Tielens, A.G.G.M. 1993, ApJ 402, 195
Wouterloot, J.G.A., Brand, J., Burton, W.B., Kwee, K.K. 1990, A&A 230, 21
Zaritsky, D., Kennicutt, R.C.Jr., Huchra, J.P. 1994, ApJ 420, 87.
Zuckerman, B., Palmer, P. 1974, ARAA 12, 279

This article was processed by the author using Springer-Verlag LaTeX A&A style file *L-AA* version 4.